Effect of microstructure on KCl corrosion attack of modified AISI 310 steel

Malede, Yohanes Chekol; Montgomery, Melanie; Dahl, Kristian Vinter; Hald, John

[Link back to DTU Orbit](#)

Effect of microstructure on KCl corrosion attack of modified AISI 310 steel

Yohanes Chekol Malede*, Melanie Montgomery, Kristian Vinter Dahl, John Hald

Department of Mechanical Engineering, Technical University of Denmark, Produktionstorvet - Building 425, DK-2800 Kgs. Lyngby, Denmark

* Email: yocmala@mek.dtu.dk

Effect of microstructure on KCl corrosion attack of modified AISI 310 steel

Abstract

The effect of microstructure on KCl corrosion attack was studied using a specifically chosen modified AISI 310 austenitic steel in a 15 % (v/v) H_2O (g) + 5 %(v/v) O_2 (g) + N_2 (g) (balance) atmosphere at 600ºC for 168h. The material was a targeted choice as it allows investigation of different microstructures i.e. as-received (without sigma phase) and heat-treated (29% σ-phase per area) microstructures. The corrosion attack was studied with light optical, scanning electron and transmission electron microscopy as well as X-ray diffraction. The heat-treated sample showed a corrosion attack that was 5 times higher than the as-received sample. In the heat-treated sample, the σ-phase was selectively attacked. At the corrosion front, chlorine (but not potassium) was detected in the selectively attacked σ- phase but not in the unattacked adjacent matrix. Therefore, the corrosion attack was propagated by preferential σ-phase attack by chlorine species.

Keywords: internal corrosion; effect of microstructure; KCl corrosion; modified 310 steel; high temperature corrosion; sigma-phase

Introduction

Power production from biomass combustion leads to severely increased corrosion of components exposed to hot flue gases compared to that observed for coal-fired boilers [1]. The higher corrosion rate in biomass power plants can be attributed to the presence of greater amounts of Cl and K in biomass than coal [2]. In biomass, alkali metals form weak organic bonds or are found in the form of simple salts [3]. Hence, they are easily released during combustion and form KCl-rich deposit on the surface of superheaters. Accordingly, many studies have been undertaken based on KCl-induced corrosion to investigate corrosion mechanisms of superheaters in biomass-firing, for

example [4–7]. The findings from [4-6] proved the reactivity of potassium with protective Cr_2O_3 to form non-protective potassium chromate.

Comparison of investigations into the effect of Cr content in the alloy to reduce corrosion in an oxidising-chloridizing environments reveals contradicting results [9]. A detrimental effect of Cr due to the formation of chromium chloride was reported at 800°C in a 50% HCl-10% H_2O-H_2 reducing atmosphere [8]. An improvement in corrosion resistance with increasing Cr content was reported in mixed oxygen-chlorine environments at 1000 °C [9]. $FeCl_2$ vapor was considered as the main corrosion product. Corrosion experiments conducted on Fe-Cr (0-25 wt.%Cr) alloys at 800°C in low HCl and low H_2O containing environments showed an improvement of corrosion resistance with increasing Cr content due to the formation of chromia [10]. From the corrosion investigation of materials from a biomass power plant, a minimum in total corrosion rate has been observed for a Cr content around 15-18 wt.%, where a high material loss was observed for lower Cr content, whilst a higher Cr content resulted in selective attack and deep internal corrosion[11]. The effect of Cr content in the alloy to improve the corrosion resistance of a material seems very specific with respect to temperature and relative partial pressures of chlorine and oxygen, as well as the chlorine species involved.

Depending on alloy composition and exposure conditions of a superheater material, the microstructure of the superheater may change with exposure time. For example, the precipitation of Cr-rich phases such as σ-phase and carbides can occur in Cr-rich superheater alloys during high temperature and long operation times [12,13]. These precipitates may affect the corrosion response of the superheater material. A preferential attack of Cr-rich carbides were also reported by Berztiss et al. [14] in a HCl environment. Based on their findings, Mo-rich carbides were more corrosion resistant

than the matrix. Grabke et al. [15] performed a corrosion test on carbide precipitates in oxidising-chloridizing atmosphere. According to their findings, $M_{23}C_6$ carbides precipitated from Fe-15%Cr-0.8% C, Fe-35%Cr-0.3% C and Fe-20%Cr-12%Ni-0.3%C alloys, were preferentially attacked when the materials were exposed to N_2-5% O_2-500-1500 vppm HCl atmosphere at 600^oC for 168h. The authors also reported a selective attack of M_7C_3 precipitates in an Fe-20Cr-33Ni-C matrix. It was concluded that the formation of chromium chloride from the reaction of chromium carbides with chlorine and oxygen was the reason for the preferential attack [15,16]. Fujikawa et al. [17] studied the corrosion behavior of austenitic stainless steels by repeated cycles of immersion in saturated chloride solution (containing mainly NaCl with a small amount of $CaCl_2$ and $CaSO_4$) followed by heating. Their results revealed that below the melting temperature of NaCl (801^OC), increasing the chromium and carbon content of the alloy increased the level of internal penetration attack. They explained their findings based on the attack of $Cr_{23}C_6$ by NaCl. However, above the melting point of NaCl, increasing Cr content of the alloy led to a decreased level of attack. They postulated that, for fused salt, the formation of chromia might control the corrosion attack. Mo_6C, TiC and NbC, prepared from Fe-15%Cr-10% Mo-0.3%C, Fe-15%Cr-5% Ti-0.3% C and Fe-18%Cr-10%Ni-0.8%Nb-0.1% C respectively, showed a better corrosion resistance than the matrix in oxidising-chloridizing atmosphere [15].

Some of the above studies were dedicated to understand the effect of Cr content to reduce the corrosion rate of materials in oxidising-chloridizing atmospheres, whilst other studies were dedicated to understand the corrosion response of carbides in oxidising-chloridizing atmospheres. However, the effect of microstructural evolution due to ageing, such as precipitation of Cr-rich phases (especially σ-phase which can form in austenitic steels with low carbon and high Cr after long exposure at high

4

temperature [13,18]), on KCl induced corrosion was not yet studied. In addition, the role of potassium in the propagation of attack after the breakdown of chromia is not understood.

The present work investigates the influence of microstructure with respect to KCl induced deposit corrosion where special emphasis is given to understanding the role of Cr rich precipitates on the extent of observed corrosion. The effect of potassium and chlorine at the propagation stage of corrosion will also be discussed. To fulfil this purpose, a modified AISI 310 austenitic steel heat-treated to contain different amounts of Cr-rich σ-phase was investigated.

Experimental procedures

Material

The investigated material was a modified AISI 310 steel with chemical composition as listed in Table 1.

Table 1. Composition of modified 310 steel

	Cr	Ni	Cu	W	Mn	C	Si	Nb	V	Ti	N	Fe
Wt.%	23.8	22.0	2.77	2.46	0.84	0.088	0.023	0.36	0.36	0.27	0.03	Balance

The material was available in three different conditions, as received (solution-treated), isothermally heat-treated in static lab air for up to 10000 hours at 650˚C and isothermally heat-treated in static lab air for up to 10000 hours at 700˚C. The material was chosen because it develops widely different microstructures depending on heat treatment, i.e. containing a large fraction of σ-phase or almost no σ-phase.

For corrosion exposures, 20mm x 8mm x 0.6 mm coupons were cut from the as received and heat-treated materials using a Struers Accutom-50 Precision Cutter. The coupons were ground with 1000-grit and 4000-grit SiC papers and cleaned with ethanol

using ultrasonic cleaning. The thicknesses of the coupons were measured using a micrometer screw with an accuracy of 0.01mm to allow evaluation of material loss after corrosion exposures.

Corrosion exposures

Exposures were done both with and without approximately 1 mm thick KCl deposit for both as received and heat-treated samples. The heat-treated condition used for corrosion testing was 700ºC for 10000 h. Application of KCl was done by dissolving KCl in isopropanol to form a semisolid mixture that was then applied to the surface of the samples followed by heating to remove the solvent.

Samples were exposed in a tube furnace equipped with a quartz tube to a 15 % (v/v) H_2O (g) + 5 %(v/v) O_2 (g) + N_2 (g) (balance) atmosphere at $600^\circ C$ for 168h. The total flow rate of the gas mixture was 200ml/min. The volumetric gas flow rates of both N_2 and O_2 were controlled via gas flow controllers, whereas the amount of water vapor was controlled by adjusting the temperature of a humidifier located before the furnace inlet. A schematic and full description of the experimental setup can be found in [19].

Preparation of cross-sections

Cross-sections of non-exposed as received and isothermally heat-treated material were produced by hot mounting in epoxy followed by grinding to 4000 grit SiC paper and polishing using 3µm and 1 µm diamond suspensions. For SEM investigation, the polished samples were etched in Kallings reagent (5g $CuCl_2$ in 100 mL hydrochloric acid and 100 mL ethanol).

Cross-sections of corrosion tested samples were cold mounted in epoxy to ensure a tight embedding and preserve the corrosion products. The sintered salt was removed before embedding to reduce the risk of smearing during grinding and

6

polishing. After preparation, neither chlorine nor potassium was observed by EDX below the area with corrosion attack, indicating that smearing was minimized. The mounted samples were ground up to 4000-grit SiC paper followed by polishing using 3µm and 1µm diamond paste and absolute ethanol (water free, 99.99%) as lubricant to reduce dissolution of the chlorine containing corrosion products.

Characterisation

Characterisation was conducted with reflected light optical microscopy (RLM), scanning electron microscopy (SEM/EDX), X-ray diffraction (XRD) and transmission electron microscopy (TEM/EDX). RLM was carried out using an Olympus CK40M microscope equipped with a Leica DFC450C camera. RLM of corrosion samples were conducted on polished samples to determine the corrosion rates and the morphologies of the corrosion products.

Before SEM investigations, samples were sputter-coated with a thin layer of carbon using a Q150R Rotary-Pump Sputter. SEM was carried out using a JEOL JSM-5900 equipped with a LaB6 filament and Oxford EDX. The EDX measurements for oxygen have a lower accuracy, and therefore the values should be assessed with caution.

XRD phase analyses were performed using a Bruker D8 Discovery diffractometer in coupled scan mode with CrKα radiation for samples before corrosion exposure. After corrosion exposure, the outer oxide was removed by polishing with 1000-grit SiC paper and MoKα radiation was used to improve the depth of penetration.

For TEM, a thin foil was prepared from the sample heat-treated at 700°C for 10000 hours both before and after corrosion exposure. The thin foil from the heat-treated sample before corrosion exposure was prepared by electropolishing using 10% perchloric acid and 10 % ethylene glycol monobutyl ether in ethanol solution at a

temperature of -20°C on a Struers Tenupol 5. FIB-milling using a FEI Helios Nanolab was used to lift out a TEM sample from the internal corrosion front from the corrosion exposed heat-treated sample. As a complement to TEM-EDX quantitative analysis, a qualitative Cr content analysis using electron energy loss spectroscopy (EELS) was performed at the corrosion front.

Thermodynamic Calculations

Thermodynamic calculations were performed using Thermo-Calc software version 2016b [20] using the Thermo-Calc Software TCFE6 Steels/Fe-alloys database version 6.1 to predict phase amounts and compositions of thermodynamically stable phases as a function of temperature.

Results

Characterisation of material before corrosion exposures

Scanning Electron Microscopy

Figure 1 shows the BSE images of as received and heat-treated samples before corrosion exposure. The microstructure of as received and heat-treated samples consists of black Ti-rich and white Nb-rich precipitates, presumably Ti(C, N), and Nb(C, N), in an austenite matrix as shown in Figure 1. The as received sample and the sample heat-treated at 650°C had no substantial amount of Cr-rich precipitates. The heat-treated sample at 700°C however, showed a very high amount of Cr rich precipitates; SEM-EDX analyses indicated that these precipitates are rich in Cr and depleted in Ni as shown in Figure 2 and correspond to σ-phase. Using quantitative image analysis, an area fraction of 0.29 for the σ-phase was measured based on analyses of five SEM BSE images as the one shown in Figure 1d.
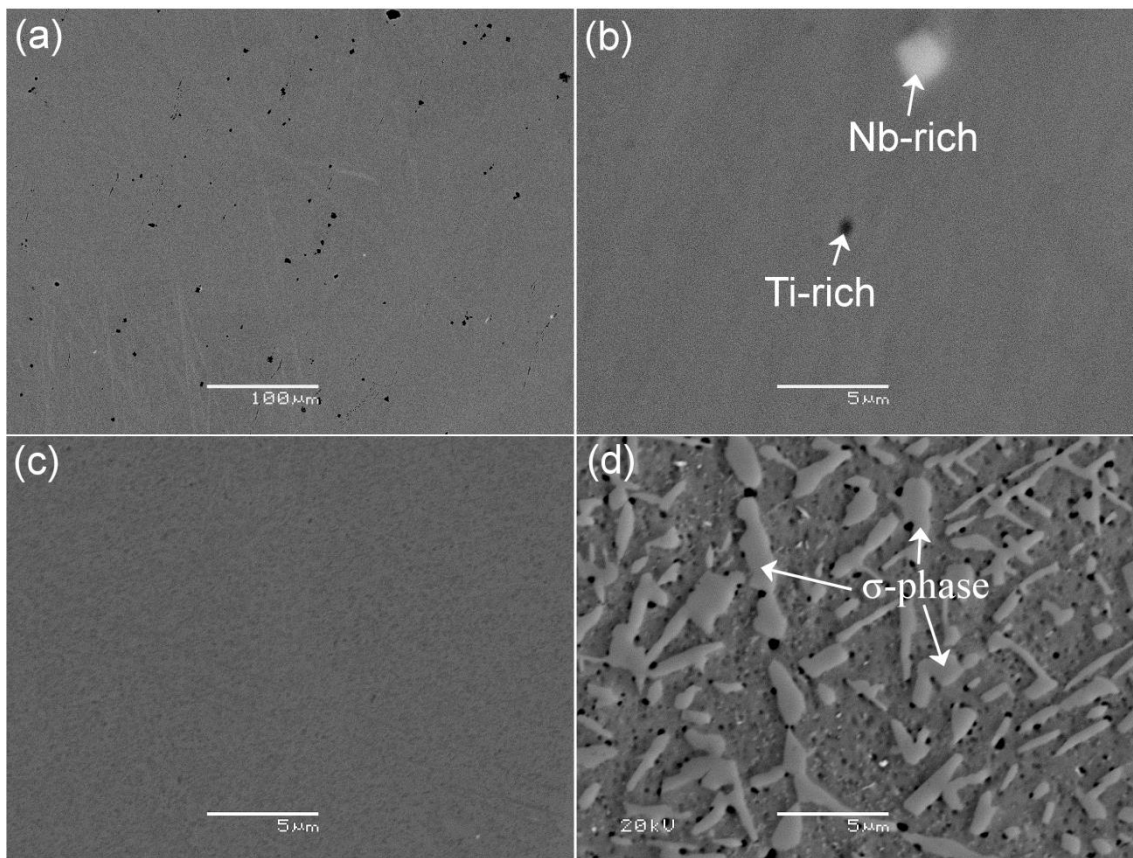
Figure 1. Microstructures of modified AISI 310 steel as (a) as received with low magnification (b) as received with higher magnification (c) heat-treated at 650^OC for 10000h (d) heat-treated at 700 $^\text{O}$C for 10000h.
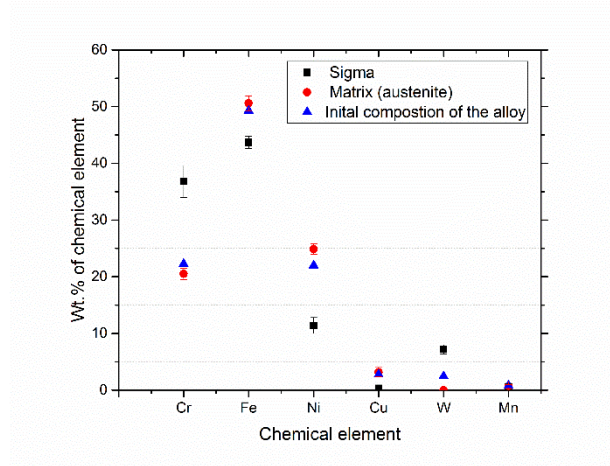
Figure 2. Initial composition of the alloy before heat treatment and compositions of austenite (matrix) and σ-phase of the heat-treated (at 700°C for 10000h) sample measured using SEM-EDX.

Transmission Electron Microscopy

TEM analysis was performed on a thin foil from the sample heat-treated at 700˚C for 10000 hours. The Cr-rich σ-phase was confirmed using electron diffraction as shown in Figure 3. The heat-treated sample did not show signs of sensitisation near to the σ-phase. Tungsten rich phases were also revealed from the TEM analysis as evidenced in Figure 3 and Table 2.

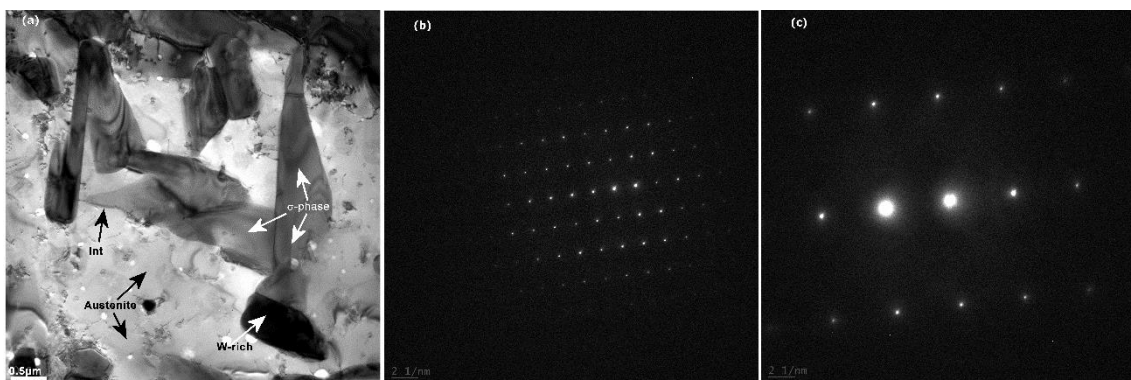Figure 3. (a) TEM micrograph of heat-treated sample on thin foils (b) Diffraction from σ-phase in [1 1 0] zone axis (c) diffraction from austenite [1 1 2] zone axis.

Table 2. TEM-EDX results in wt. % for regions shown in Figure 3a.

Composition (Wt. %)	Cr	Fe	V	Mn	Ni	Nb	W
Austenite	21.3	52.1	0.4	1.1	25.2	-	-
σ-phase	43.8	38.8	0.3	0.6	7.5	-	9.1
Near to interface (Int)	21.7	51.5	0.3	0.9	25.7	-	-
W-rich phase	14.0	25.0	-	0.5	5.1	1.5	53.9

X-ray Diffraction

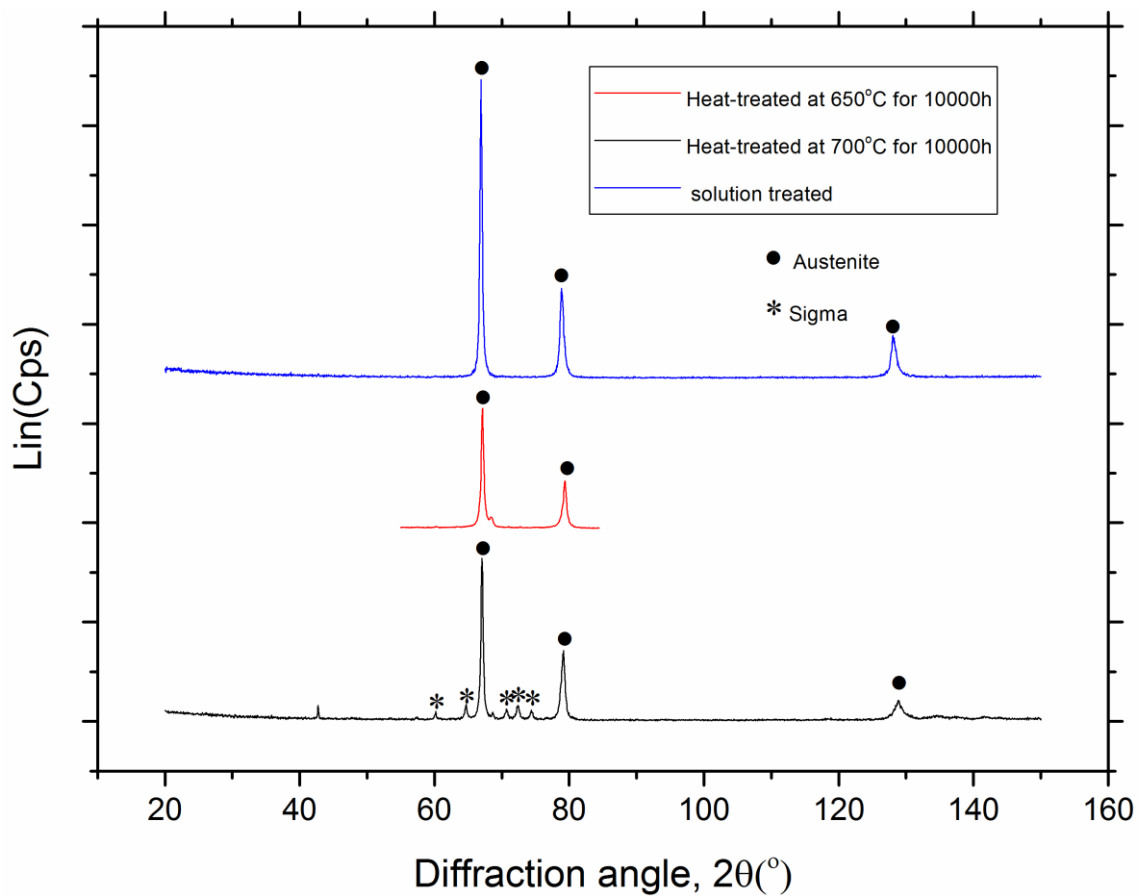The XRD results confirmed that the Cr-rich precipitates shown in Figure 1c are σ-phase, (Figure 4).

Figure 4. XRD analysis for modified AISI 310 austenitic steel in the as received and heat-treated conditions.

Thermodynamic Calculation

The equilibrium phases in modified AISI 310 austenitic steel are shown in Figure 5. Austenite and σ-phase are the most significant thermodynamically stable phases predicted by Thermo-Calc between 500ºC and 800ºC. The equilibrium volume percent of σ-phase calculated using Thermo-Calc at 700ºC was 26 %. The equilibrium composition of σ-phase calculated using Thermo-Calc is tabulated in Table 3.
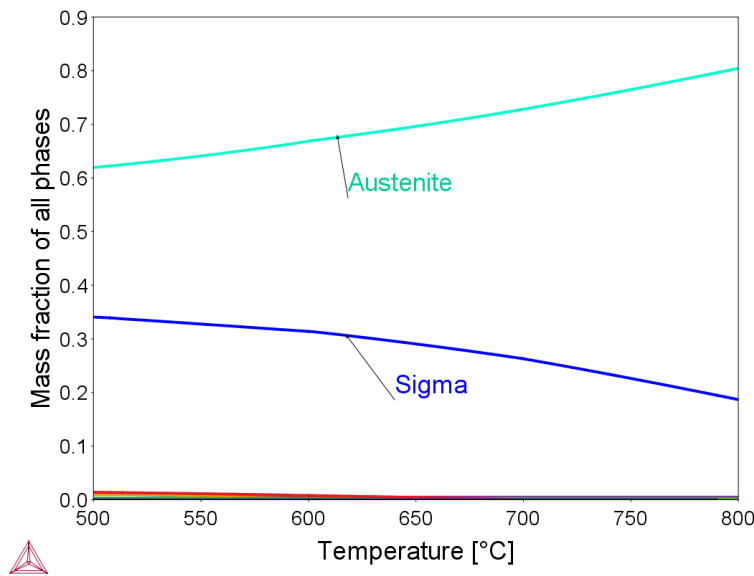

Figure 5. Equilibrium phases in modified AISI 310 austenitic steel

Table 3. The equilibrium composition of σ-phase at 700ºC for a modified AISI 310 steel calculated using Thermo-Calc.

Composition (Wt. %)	Cr	Fe	V	Ni	W
σ-phase	44.6	40.4	0.4	7.4	7.2

Characterisation of materials after corrosion testing

Light Optical Microscopy

Figure 6 shows RLM images of the corrosion tested steel in both as received and heat-treated condition, exposed both with and without the presence of KCl. Selective internal corrosion was observed for the heat-treated sample in both KCl-free and KCl-bearing

exposures. In the KCl-free exposure, the heat-treated sample showed an increased corrosion attack compared to the as received sample. However, in the presence of KCl a drastic increase in corrosion attack was observed for the heat-treated sample both compared to the reference exposure and compared to the as received sample exposed in the presence of KCl.
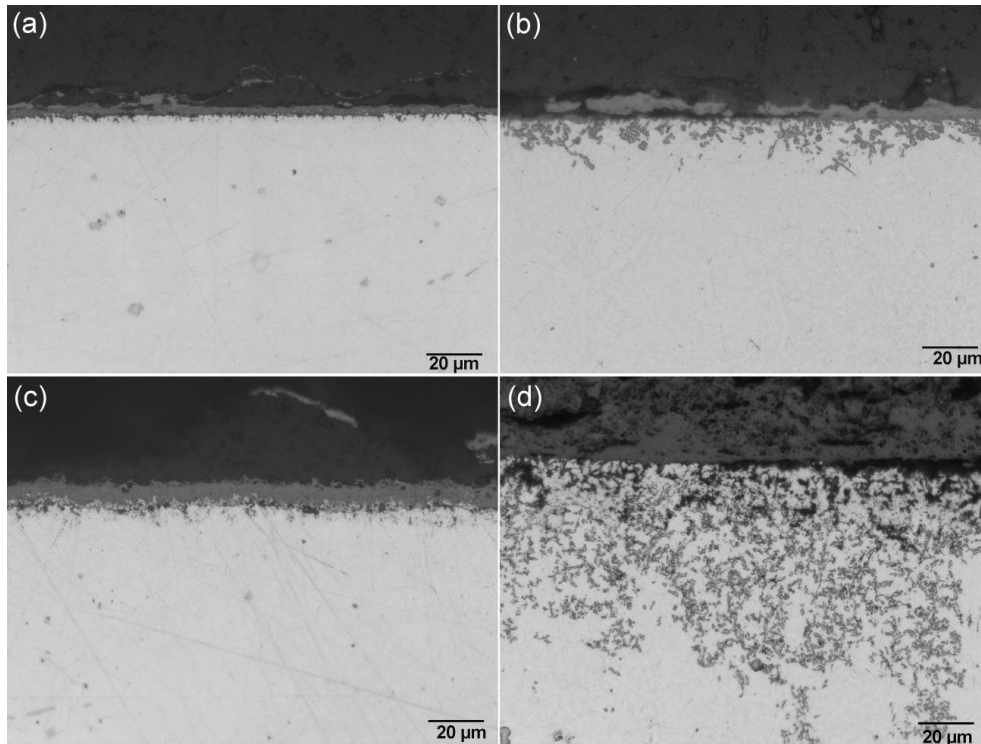

Figure 6. RLM micrographs after exposure in a 15 % (v/v) H_2O (g) + 5 %(v/v) O_2 (g) + N_2 (g) (balance) atmosphere at 600°C for 168h. (a) as received KCl-free sample (b) heat-treated KCl-free sample (c) as received covered with KCl sample (d) heat-treated covered with KCl sample.

The total corrosion attack measured from residual metal thickness of the heat-treated and as received samples are presented in Figure 7. The lines in the box chart, from bottom to top, represent the 5th, 25th, median, 75th and 95th percentiles and the square in the chart represent the mean value. The minimum and the maximum values are represented by (x).
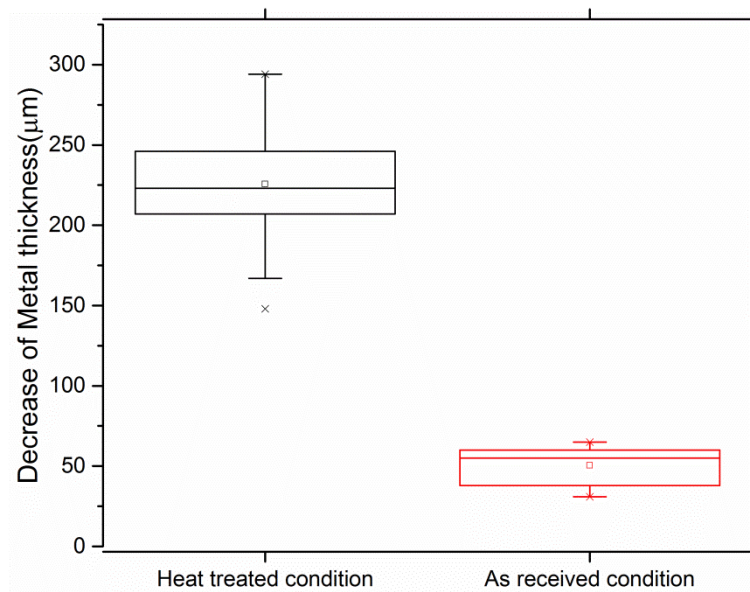
Figure 7. Corrosion rates of heat-treated and as received samples covered with KCl and exposed at 600°C for 168h to 15 % (v/v) H_2O (g) + 5%(v/v) O_2 (g)+ N_2 (g) (balance) atmosphere.

As it is clearly seen in Figure 7, the heat-treated sample showed higher depth of attack and the values had a large scatter compared to the as received sample. The higher deviation of the corrosion attack in the heat-treated sample is due to the nature of the corrosion attack see Figure 6d. While a selective type of internal attack was observed in the heat-treated sample, the untreated sample showed a uniform type of attack.

Scanning Electron Microscopy

*Corrosion of the as received sample in KCl bearing environment.*The BSE images in Figure 8 show the presence of an outer oxide layer and internal attack for the material tested in as received condition exposed to KCl. The as received sample showed an iron-rich mixed outer oxide layer (53.5 wt. % Fe, 18 wt. % Cr, 2.6 wt. % Ni and balance oxygen). The bright phase in Figure 8b is a Ni-rich phase.
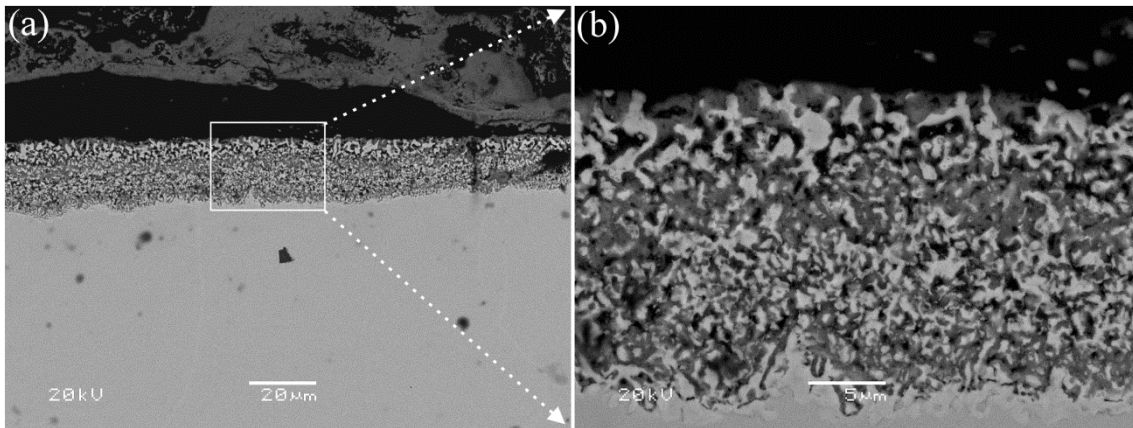
Figure 8. BSE images for (a) the as received sample covered with KCl and exposed in 15 % (v/v) H_2O (g) + 5 %(v/v) O_2 (g) + N_2 (g) (balance) atmosphere at 600°C for 168h (b) KCl exposed as received sample at higher magnification as marked in (a)

A closer look at the internal corrosion of the as received and heat-treated samples shows a striking difference, not only in terms of the severity of corrosion attack but also with respect to morphology. A uniform type of internal corrosion attack was observed at the corrosion front for the as received sample (Figure 8a and 8b).

EDX mapping at the corrosion front (internal corrosion) for the as received sample after corrosion testing indicated the presence of Ni bands as depicted in Figure 9. Ni-enrichment was observed at the corrosion front.

Figure 9. EDX mapping at the corrosion front for the as received sample, after corrosion exposure in KCl bearing environment.

Corrosion of the heat-treated sample in KCl bearing environment. EDX analysis showed that the outer oxide layer in the case of the heat-treated sample revealed distinct Fe-rich (71.5wt. % Fe , 0.8 wt. % Cr and balance oxygen) and Cr-rich (66.1 wt.% Cr, 1.7wt.% Fe and balance oxygen) regions. The heat-treated samples developed much thicker external oxides and also higher internal corrosion than the as received sample as shown in Figure 10 and Figure 8a.
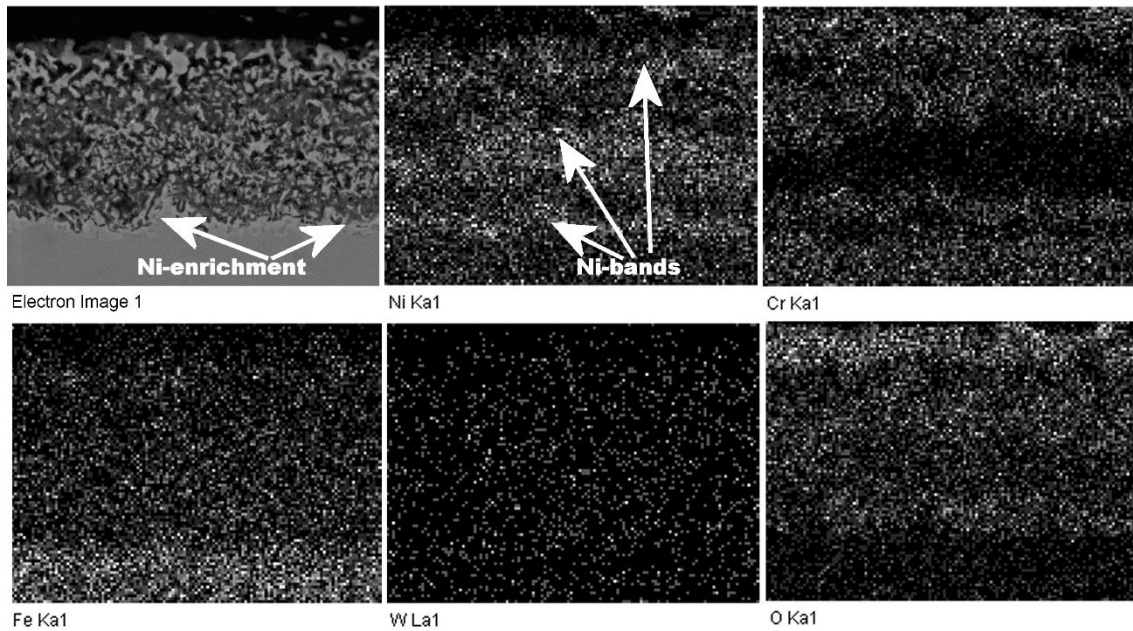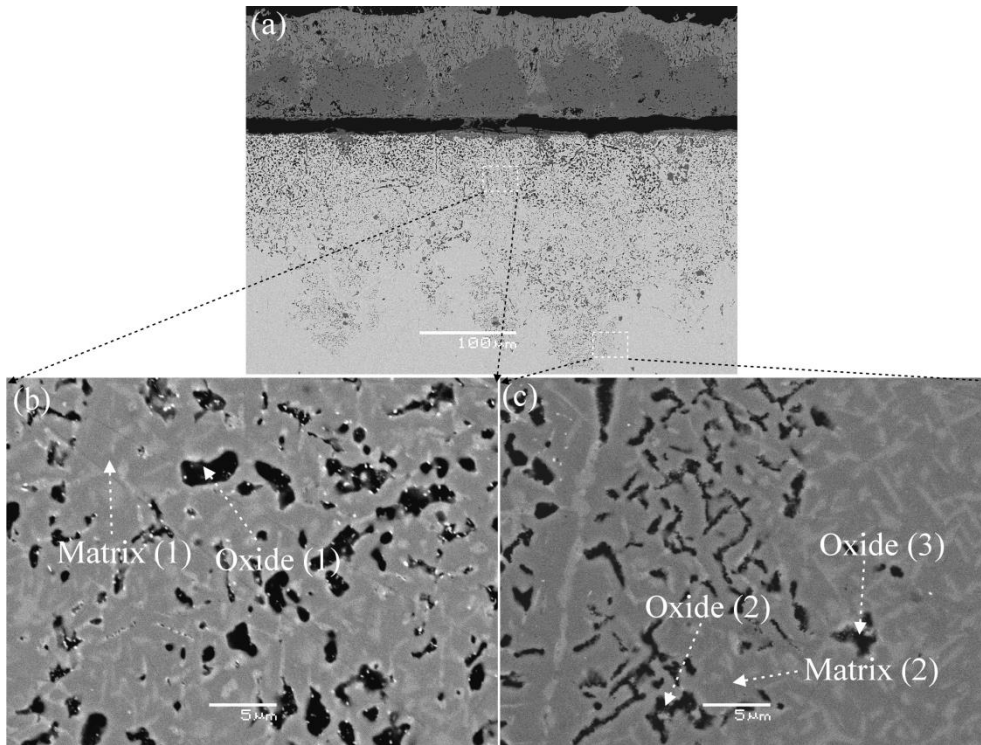
Figure 10. BSE images for (a) the heat-treated sample covered with KCl and exposed in 15 % (v/v) H_2O (g) + 5 %(v/v) O_2 (g) + N_2 (g) (balance) atmosphere at 600°C for 168h. (b) corrosion 'within' the internal corrosion zone with higher magnification (c) the 'corrosion front' at higher magnification. In (b) and (c) σ-phase was selectively attacked. EDX analysis locations according to Table 4 are marked.

The internal corrosion attack in the heat-treated sample was of a more selective type as indicated in Figure 10b and Figure 10c where the σ-phase was preferentially attacked. The bright small precipitates in Figure 10b are Nb-rich phases. At the corrosion front, the corrosion attack of the heat-treated sample showed a similar morphology with that of σ-phase, (see Figure 10c). A pronounced corrosion attack was observed in regions that may have had interconnection along σ-phases as shown in Figure 10c.

A local EDX analysis on the heat-treated sample, 'within' the internal corrosion zone, see locations in Figure 10, showed strong chlorine and relatively weak potassium

signals within the oxide but no such signal in the unattacked matrix (see compositions of oxide (1) and matrix(1) in Table 4). Care must be taken in the interpretation of these measurements, as the analysis in some areas is where there are apparent voids, and therefore analysis of the underlying region is undertaken.

Table 4. EDX investigation for areas shown in Figure 10.

Composition (Wt. %)	O	Cl	K	Cr	Fe	Ni	Cu	W
Matrix (1)	-	-	-	17.9	50.9	31.2	-	-
Oxide (1)	21.0	7.6	1.1	7.0	30.7	23.4	3.3	6.0
Matrix (2)	-	-	-	20.1	51.9	24.8	3.2	-
Oxide (2)	11.8	2.3	-	16.2	38.5	18.8	2.3	10.0
Oxide (3)	4.77	8.0	-	17.6	40.8	18.4	3.2	7.2

At the corrosion front, while a strong signal of chlorine was observed in the oxide, there was no indication of chlorine signal in the unattacked matrix, see compositions of matrix(2) and oxide(2) and oxide(3) in Table 4. Potassium was not detected either in the matrix or in the oxide at the corrosion front.

Transmission Electron Microscopy

The TEM investigation of the corrosion exposed heat-treated sample revealed that the chromium content of the oxide at the corrosion front is lower than the chromium content of the nearby matrix as shown in Table 5 and Figure 11c. The chromium content near to the oxide increases with increasing distance from the oxide while the opposite effect was observed for nickel. Similar to the SEM investigation, chlorine was observed in the oxide but not in the matrix and a lower Cr content was measured compared to the original σ-phase.

Table 5. TEM EDX analysis for heat-treated corrosion exposed sample shown in Figure 11a and 11b.

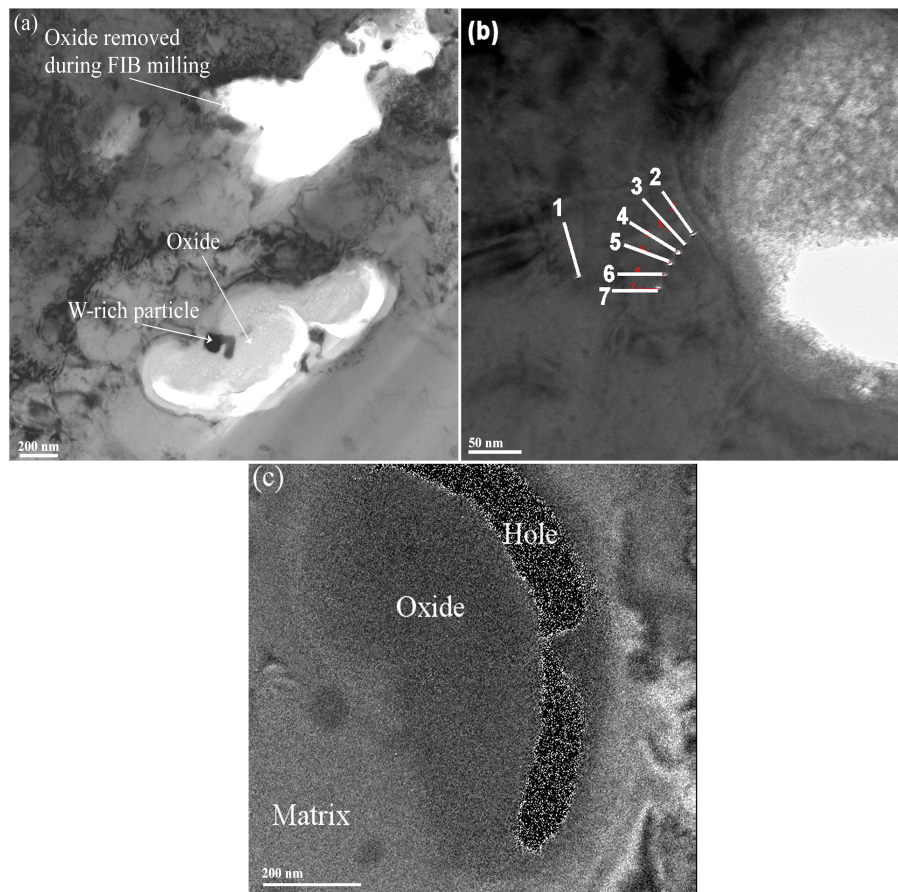| Composition (Wt. %)	O	Mn	Cl	Cr	Fe	Ni	W
Oxide	24.2	-	4.4	6.5	16.7	33.1	15.1
1	-	-	-	20.4	52.8	26.8	-
2	-	0.76	-	15.8	54.0	29.4	-
3	-	-	-	17.8	55.1	27.1	-
4	-	-	-	18.8	54.8	27.1	-
5	-	-	-	19.4	54.2	26.3	-
6	-	-	-	19.9	53.6	26.4	-
7	-	-	-	20.2	53.2	26.6	-

Figure 11. TEM bright field micrographs of thin foil at the corrosion front for the heat-treated sample covered with KCl and exposed in 15 % (v/v) H_2O (g) + 5%(v/v) O_2 (g)+

N$_2$ (g) (balance) atmosphere at 600°C for 168h. (a) Oxide (b) TEM-EDX analysis near to oxide (c) Qualitative Cr content analysis in the oxide and near to the oxide using electron energy loss spectroscopy (EELS). Dark regions are lower in Cr content .

X-ray Diffraction

To investigate the internal oxide of the heat-treated sample that was exposed in a KCl bearing environment, the outer oxide was removed by polishing using 1000-grit SiC paper. The XRD investigation of the heat-treated corrosion exposed sample is presented in Figure 12. The XRD result showed the presence of austenite, $(Fe,Cr)_3O_4$ and $(Fe, Cr)_2O_3$ phases but not σ-phase, although σ-phase was detected in the heat-treated sample before corrosion exposure. The absence of σ-phase indicates the selective attack of σ-phase compared to the matrix (austenite).The Nb-rich and Ti-rich phases were not detected probably because their volume fraction were below the detection limit of the XRD.
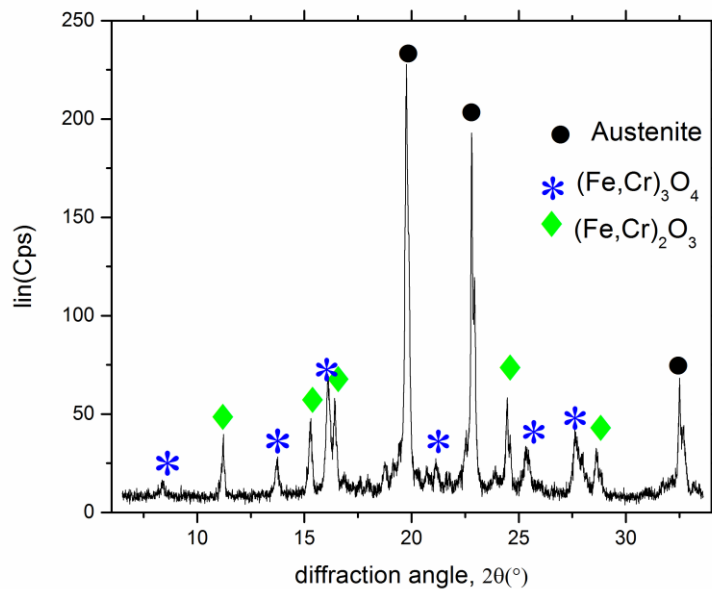

Figure 12. XRD analysis for the heat-treated sample covered with KCl and exposed in 15 % (v/v) H$_2$O (g) + 5 %(v/v) O$_2$ (g) + N$_2$ (g) (balance) atmosphere at 600°C for

168h. The outer oxide layer was removed using 1000-grit SiC before the XRD measurement. Austenite was observed but not σ-phase.

Discussion

Influence of heat treatment

The modified AISI 310 steel allowed the corrosion investigations of two widely different microstructural conditions. This was done by selecting a suitable material based on thermodynamic and kinetic considerations. A heat-treatment of the modified AISI 310 austenitic steel at 650^OC for 10000 h did not yield a significant amount of precipitation of σ-phase, Figure 1, whereas, heat-treatment at 700^OC for 10000 h gave a significant precipitation of σ-phase (29% σ-phase per area). As the corrosion experiments were conducted at $600^°$C for 168h, which is at a lower temperature and shorter time compared to a heat treatment at $650^°$C for 10000 h, then, it would be expected that σ-phase does not form during corrosion testing of the material in as received condition. Furthermore, σ-phase is thermodynamically stable at $600^°$C as shown in Figure 5. Hence, it can be expected that σ-phase will not be dissolved in the $700^°$C heat-treated sample during corrosion testing at $600^°$C. Thus, formation or dissolution of notable amounts of σ-phase is not expected during corrosion testing. In effect, this made it possible to corrosion test material with the same overall composition but with widely different microstructures; i.e. no σ-phase and 29% σ-phase per area. The outputs of the heat treatments and the selection of the temperature of the corrosion test allow comparison of the same steel with the same composition in heat-treated (which could be taken as ageing in a high temperature power plant) and as received condition.

The predicted equilibrium composition of σ-phase at 700°C using Thermo-Calc software is tabulated in Table 3; the result is in good agreement with TEM-EDX results of σ-phases as shown in Table 2 and SEM/EDX, Figure 2. As compared to the matrix, σ-phase is rich in chromium and tungsten but lean in nickel. Due to the higher amount of chromium content in σ-phase, chromium depletion could be expected near to σ-phase. Nevertheless, comparison of TEM-EDX results in the matrix near to the interface of σ-phase indicated the absence of sensitisation near to σ-phase; cf. Table 2. This is probably due to a high mobility of chromium at 700°C from the matrix towards the sigma-matrix interface to avoid depletion. Since the heat-treated sample was treated at 700°C for longer times (10000 h), any sensitised areas will be expected to obtain Cr from the matrix and depletion gradients will disappear (be healed). Tavares et al. [21] reported a short time sensitisation for AISI 310 steel heat-treated at 700°C, which was then removed after around 100 h heat treatment . Tungsten rich phases were also revealed from the TEM analysis as evidenced in Figure 3. This could be Laves phase or W(bcc), but it was not further investigated.

Corrosion testing

External oxide scale

Although the average composition of the heat-treated and as received samples were similar, the heat-treated sample showed a strikingly higher corrosion attack than the as received sample in the KCl bearing environment due to the presence of σ-phase in the former, see Figure 6. The outer oxide of the heat-treated sample in the KCl bearing environment consists of Fe-rich and Cr-rich oxides. Previous studies on Fe18Cr10Ni steel at 600 °C in KCl containing environments showed an outward growing Fe-rich hematite (α-Fe_2O_3) and an inward growing Cr-rich $(Fe,Cr)_3O_4$ spinel [6,22]. Jonsson et

al. [23] explained the formation of outer Fe-rich oxide layer by the higher diffusivity of Fe^{2+} than Cr^{3+} in the spinel. According to Grabke et al. [15] the positions of oxides in oxidising-chloridizing atmosphere can be explained based on the oxygen partial pressure required to convert the evaporating metal chlorides into oxide. The lower the value of this critical P_{O2}, the smaller the distance the chloride needs to move from the corrosion front before it converts into oxide. A higher oxygen partial pressure is needed to convert iron chloride than chromium chloride into the respective oxides. Accordingly, Fe-rich oxide was formed at the outer part of the external oxide scale and Cr-rich oxide was formed in the internal part of the outer oxide scale. This is in good agreement with the external oxide of the heat-treated sample. The as received sample exposed with KCl showed relatively thinner external oxide than the heat-treated sample exposed to the same condition. The fact that Cr and Fe oxide are present gives an indication that these elements have been removed from the alloy.

Internal corrosion

The heat-treated sample showed a significantly higher internal corrosion compared to the as received sample in the KCl bearing environment due to the presence of σ-phase in the heat-treated sample. The Ni-enrichment at the corrosion front (see Figure 9) could also play a role in decreasing the internal corrosion of the as received sample as Ni has low affinity to both chlorine and oxygen [15]. Interestingly, the samples revealed quite different internal corrosion morphologies. While the as received sample showed a 'uniform' type of internal corrosion morphology, the heat-treated sample showed a 'selective' type of internal corrosion as shown in Figure 8 and Figure 10 respectively. In the internal corrosion zone of the heat-treated sample, austenite, $(Fe,Cr)_2O_3$ and $(Fe,Cr)_3O_4$ phases were identified through XRD as shown in Figure 12. The absence of

23

the σ-phase and the presence of the austenite (matrix) confirms the selective attack of the σ-phase. A selective attack of Cr-rich $M_{26}C_6$ and M_3C_7 precipitates was reported in chlorine containing environments by Grabke et al. [15] and Fujikawa et al. [17]. On the other hand, the Nb-rich precipitate showed a good corrosion resistance as shown in Figure 10b. Mo_6C, TiC and NbC were reported as being more corrosion resistant than the matrix in oxidising-chloridizing atmosphere [15].

Sensitisation (due to the precipitation of σ-phase) and / or volatile chromium chloride formation (from the reaction of Cr-rich σ-phase with chlorine) could be reasons for the observed higher, selective type of, corrosion attack of the heat-treated sample in KCl bearing environments. As σ-phase is a Cr rich phase, precipitation of σ-phase from the matrix may lead to a Cr depleted zone (sensitisation) near to σ-phase. If the Cr content is below 12 wt.%, a protective passive film cannot readily form [24]. Nevertheless, the TEM-EDX analysis showed that there was no measurable sensitisation near to the σ-phase in the heat-treated sample before corrosion exposure as shown in Table 4. Hence, the selective attack and higher corrosion attack in the heat-treated sample in KCl bearing environment cannot be explained based on the mechanism of sensitisation.

The other postulated mechanism for the observed significantly higher selective internal attack of the heat-treated sample in KCl bearing environments was based on the reaction of chromium rich σ-phase with chlorine to easily form Cr-rich volatile chloride followed by formation of oxide through active oxidation [3,15,25] and/or ionic transport [26,27] . The preferential chlorine attack of Cr rich phases is substantiated by the following observations.

- The significantly higher corrosion attack of the heat-treated sample in KCl bearing environments as compared to KCl-free environment, cf. Figure 6b and Figure 6d.

- The preferential attack of the chromium rich σ-phase (see Figure 10) as compared to the relatively lower chromium content matrix.

- The presence of significant amount of chlorine in the internal corrosion zone and at the corrosion front. The chlorine signal was observed only in the selectively corroded σ-phase but not in the unattacked matrix as shown in Table 4.

- A pronounced corrosion attack was observed in regions that had good interconnection among σ-phases as shown in Figure 10c.

- The depth of the corrosion attack and the formation of porous corrosion product suggests that attack occurs due to a gas phase reaction.

- The selectively attacked internal oxide of the heat-treated sample had low Cr content (see Table 5), although the initial σ-phase, from which the internal oxide was formed, was rich in Cr. This implies the volatility of chromium from σ-phase perhaps in the form of chromium chloride. This chromium chloride is then oxidized and forms the external oxide.

- The matrix, adjacent to the preferentially attacked oxide, showed a progressive depletion in Cr content towards the oxide as shown in Table 5. This suggests the diffusion of Cr from the adjacent matrix towards the reaction zone.

These observations reveal preferential attack of Cr rich sigma phase by chlorine species, where the Cr and Fe chloride then evaporates and is oxidised closer to the surface where there is higher partial pressure of oxygen.

Role of potassium and chlorine in the corrosion attack

Both potassium and chlorine signals were detected near the external oxide – internal oxide interface as shown in Figure 10a. Both potassium and chlorine were found in the selectively attacked oxide but not in the nearby matrix. However, closer to the corrosion front, only a strong signal of chlorine was observed. Likewise, the chlorine was found in the oxide but not in the nearby matrix. Hence, it can be concluded that, the corrosion reaction was mainly propagated because of chlorine, not because of potassium. The role of potassium seems only to contribute in the initial breakdown of the protective oxide layer. The initial destruction of the protective oxide scale by forming potassium chromate was reported by Li et.al [28] and Pettersson et al. [26].

The presence of Cr-rich phases such as σ-phase and Cr-rich carbides increases the corrosion attack of materials exposed to high temperature in chlorine containing environments such as a biomass boiler. Hence, the usage of high amounts of Cr that might lead to precipitation of Cr-rich phases during high temperature and long service times should be avoided. However, at low temperatures where no precipitates are formed, increased Cr may be beneficial.

Conclusions

- Modified AISI 310 steel allowed the corrosion investigation of the same steel composition in two widely different microstructural conditions.

- Both heat-treated and as received samples showed an increase in corrosion attack with KCl. However, the presence of KCl drastically increased the corrosion attack of heat-treated sample and selective attack was observed for such sample due to the presence of Cr-rich σ-phase.

- Therefore, corrosion attack in KCl bearing environments is not only due to the amount of Cr within the steel, but the actual microstructure of the steel with respect to Cr distribution.

Acknowledgments

References

[1]   Coleman KE, Simms NJ, Kilgallon PJ, et al. Corrosion in Biomass Combustion Systems. Mater. Sci. Forum. 2008;595:377–386.

[2]   Blomberg T. Which are the right test conditions for the simulation of high temperature alkali corrosion in biomass combustion? Mater. Corros. 2006;57:170–175.

[3]   Nielsen HP, Frandsen FJ, Dam-Johansen K, et al. Implications of chlorine-associated corrosion on the operation of biomass-fired boilers. Prog. Energy Combust. Sci. 2000;26:283–298.

[4]   Kiamehr S, Dahl K V, Lomholt TN, et al. High Temperature Corrosion due to Biomass Firing : A Study on the Reactivity between Potassium Chloride and Oxides. Int. Symp. High-temperature Oxid. Corros. 2014;144–147.

[5]   Pettersson C, Pettersson J, Asteman H, et al. KCl-induced high temperature corrosion of the austenitic Fe-Cr-Ni alloys 304L and Sanicro 28 at 600 ℃. Corros. Sci. 2006;48:1368–1378.

[6]   Jonsson T, Froitzheim J, Pettersson J, et al. The influence of KCl on the corrosion of an Austenitic stainless steel (304L) in oxidising humid conditions at 600℃: A microstructural study. Oxid. Met. 2009;72:213–239.

[7]   Okoro SC, Kiamehr S, Montgomery M, et al. Effect of flue gas composition on deposit induced high temperature corrosion under laboratory conditions mimicking biomass firing. Part II: Exposures in SO2 containing atmospheres. Mater. Corros. 2017; 68(5) :491–508.

[8]   Chu H, Datta P, Strafford K. Corrosion behavior of Fe (Ni) CrAlX alloys in an HCl− H2O− H2 gas mixture at 800° C. Oxid. Met. 1995;43:491–508.

[9]   Strafford KN, Datta PK, Forster G. High-temperature chloridation of binary FeCr alloys at 1000 °C. Mater. Sci. Eng. A. 1989;120:61–68.

[10]   Zheng X, Rapp R A. Chloridation-oxidation of Fe-Cr and Ni-Cr alloys at 800°C. Oxid. Met. 1997;48:527–551.

[11]   Montgomery M, Karlsson A. In-situ corrosion investigation at Masnedø CHP plant – a straw-fired power plant. Mater. Corros. 1999;50:579–584.

[12]   Kina AY, Souza VM, Tavares SSM, et al. Microstructure and intergranular corrosion resistance evaluation of AISI 304 steel for high temperature service. Mater. Charact. 2008;59:651–655.

[13]   Hsieh C-C, Wu W. Overview of Intermetallic Sigma Phase Precipitation in Stainless Steels. ISRN Metall. 2012;2012:1–16.

[14]   Berztiss D, Zahs A, Schneider A, et al. Role of carbides in the high temperature corrosion of steels in HCl-containing atmospheres. Zeitschrift für Met. 1999;90:4–12.

[15]   Grabke HJ, Spiegel M, Zahs A. Role of alloying elements and carbides in the chlorine-induced

corrosion of steels and alloys. Mater. Res. 2004;7:89–95.

[16]   Bender R, Schütze M. The role of alloying elements in commercial alloys for corrosion resistance in oxidising-chloridizing atmospheres part I: Literature evaluation and thermodynamic calculations on phase stabilities. Mater. Corros. 2003;54:567–586.

[17]   Fujikawa, H. and NM. Corrosion behaviour of austenitic stainless steels in the high chloride-containing environment. Mater. Sci. Eng. 1989; 120:301–306.

[18]   Sourmail T. Precipitation in creep resistant austenitic stainless steels. Mater. Sci. Technol. 2001;17:1–14.

[19]   Kiamehr S, Dahl K V., Montgomery M, et al. KCl-induced high temperature corrosion of selected commercial alloys: Part II: Alumina and silica-formers. Mater. Corros. 2016;67:26–38.

[20]   Andersson JO, Helander T, Höglund L, et al. Thermo-Calc & DICTRA, computational tools for materials science. Calphad Comput. Coupling Phase Diagrams Thermochem. 2002;26:273–312.

[21]   Tavares SSM, Moura V, da Costa VC, et al. Microstructural changes and corrosion resistance of AISI 310S steel exposed to 600-800°C. Mater. Charact. 2009;60:573–578.

[22]   Karlsson S, Pettersson J, Johansson LG, et al. Alkali Induced High Temperature Corrosion of Stainless Steel: The Influence of NaCl, KCl and $CaCl_2$. Oxid. Met. 2012;78:83–102.

[23]   Jonsson T, Karlsson S, Hooshyar H, et al. Oxidation After Breakdown of the Chromium-Rich Scale on Stainless Steels at High Temperature: Internal Oxidation. Oxid. Met. 2016;85:509–536.

[24]   Tedmon CS, Vermilyea DA, Rosolowski JH. Intergranular Corrosion of Austenitic Stainless Steel. 1971;118:192–202.

[25]   O'Hagan CP, O'Brien BJ, Leen SB, et al. A microstructural investigation into the accelerated corrosion of P91 steel during biomass co-firing. Corros. Sci. 2015;109:101–114.

[26]   Pettersson J, Asteman H, Svensson JE, et al. KCl induced corrosion of a 304-type austenitic stainless steel at 600°C; the role of potassium. Oxid. Met. 2005;64:23–41.

[27]   Folkeson N, Jonsson T, Halvarsson M, et al. The influence of small amounts of KCl(s) on the high temperature corrosion of a Fe-2.25Cr-1Mo steel at 400 and 500°C. Mater. Corros. 2011;62:606–615.

[28]   Li YS, Spiegel M, Shimada S. Corrosion behaviour of various model alloys with NaCl-KCl coating. Mater. Chem. Phys. 2005;93:217–223.